LIMNOLOGY and OCEANOGRAPHY: METHODS



Limnol. Oceanogr.: Methods 22, 2024, 527–535
© 2024 The Author(s). Limnology and Oceanography: Methods published by
Wiley Periodicals LLC on behalf of Association for the Sciences of
Limnology and Oceanography.
doi: 10.1002/lom3.10625

Small-scale measurement of fracture toughness of muddy marine sediments via bubble injection

Anika S. Cho, 1,2 Kelly M. Dorgan 0,1,3 Grant Lockridge 1,4

Abstract

Muddy marine sediments are elastic materials in which bubbles grow and worms extend their burrows by fracture. Bubble growth and burrowing behavior are dependent on the stiffness and fracture toughness (K_{Ic}) of these muds. This article describes a custom laboratory apparatus to measure the fracture toughness of muddy, cohesive sediments using a bubble injection method. The system induces fracture in sediment samples by incrementally injecting air through a needle inserted into the sediment. The increasing pneumatic pressure is monitored until it drops abruptly, indicating bubble formation. Fracture toughness is then calculated from the peak pressure at which fracture occurred, following cavitation rheology methods developed for soft gels. The system has produced measurements that compare well to previous data but with better spatial resolution, allowing for characterization of spatial heterogeneity on small scales.

Muddy marine sediments cover \sim 70% of the Earth's surface, provide habitats for diverse and abundant fauna, and are important sites for the deposition and burial of organic matter (Meysman et al. 2006). Bioturbation, the mixing of sediments by organisms, is a key contributor to benthic ecosystem health, promoting microbial productivity, nutrient cycling, and oxygen distribution (Meysman et al. 2006). The mechanisms by which burrowing organisms, such as worms and other infauna, contribute to bioturbation are not well understood, however.

In cohesive sediments, burrows extend by fracture (Dorgan et al. 2005). Fracture toughness ($K_{\rm Ic}$), the material property that characterizes the resistance of a material to fracture, is important in understanding this small-scale physical process. A higher fracture toughness indicates that more energy must be exerted by organisms to extend their burrows (Dorgan et al. 2011). Fracture toughness also affects microcracking and crack branching, which have been suggested to contribute to bioturbation by freeing particles from the cohesive matrix (Dorgan and Arwade 2023). Measurements of fracture toughness therefore provide insights into how burrowing behaviors

*Correspondence: kdorgan@disl.org

Additional Supporting Information may be found in the online version of this article.

This is an open access article under the terms of the Creative Commons Attribution-NonCommercial License, which permits use, distribution and reproduction in any medium, provided the original work is properly cited and is not used for commercial purposes.

and bioturbation activity may vary in response to different sediment properties.

Bubbles also grow by fracture in cohesive sediments; higher fracture toughness indicates that greater pressures are required for bubbles to grow (Johnson et al. 2002). X-ray CT images show disk-shaped bubbles, and pressure measured from growing bubbles drops in discrete increments consistent with fracture (Boudreau et al. 2005; Boudreau 2012). This mechanism of bubble growth applies when bubbles are at least several times larger than grain size, and when sediments are cohesive rather than fluid or granular (Boudreau 2012). Thus, fracture toughness is an important metric in predicting the transport and release of gas bubbles from sediments, e.g., of methane produced by anaerobic microbes or dissociation of methane hydrates (Boudreau 2012; Daigle et al. 2020).

There have been only a few measurements of fracture toughness in natural sediments, and more data are needed to determine how fracture toughness varies across different sediment types. Johnson et al. (2002) injected bubbles through the bottom of muddy sediment cores and of seawater gelatin, which exhibited similar fracture behavior. As air was gradually injected, bubble growth could be observed as stepwise drops in pressure corresponding to increases in bubble volume. Measurements of pressure and bubble volume were related to calculate $K_{\rm Ic}$ following the ideal gas law (Johnson et al. 2002). This method was time-consuming, limited in spatial coverage, and required bringing sediments back to the lab. To address these problems, Johnson et al. (2012) developed an in situ probe to measure fracture toughness. Their corkscrew-shaped

¹Dauphin Island Sea Lab, Dauphin Island, Alabama, USA

²Department of Electrical and Computer Engineering, University of Alabama, Tuscaloosa, Alabama, USA

³Stokes School of Marine and Environmental Sciences, University of South Alabama, Mobile, Alabama, USA

⁴Naval Research Laboratory, Stennis Space Center, Mississippi, USA

probe is rotated down into the sediment and pulls up to drive a crack inward across a plug of sediment. $K_{\rm Ic}$ is calculated from the upward force using theory of fracture across the minimum diameter of a screw (Johnson et al. 2012). Dorgan et al. (2024) have identified and resolved several problems with this design and expanded its use to characterizing the limit of sediment cohesion. However, the resulting fracture toughness greatly increases in magnitude and indicates increasing ductility with depth in sediment (Dorgan et al. 2024), which is inconsistent with fracture mechanics theory and the results from Johnson et al. (2002).

Recent advances in measuring fracture toughness in soft gels have potential implications for improved measurements of fracture toughness in sediments. The field of cavitation rheology uses the formation of cavitation bubbles to measure physical properties of soft materials for which traditional mechanical testing methods do not work well (Barney et al., 2022). Needle-induced cavitation, in which a needle punctures a soft material and a pressurized fluid (air or water) is injected, results in the growth of a disk-shaped crack rather than a spherical cavitation bubble when the initial size is large enough and/or the material is stiff enough (Kundu and Crosby 2009; Hutchens et al. 2016). The implications of this work are that fracture toughness can be calculated from the initial pressure at which a crack-shaped bubble forms, which is a much simpler and more localized measurement than the repeated crack growth events needed to calculate fracture toughness following the methods of Johnson et al. (2002).

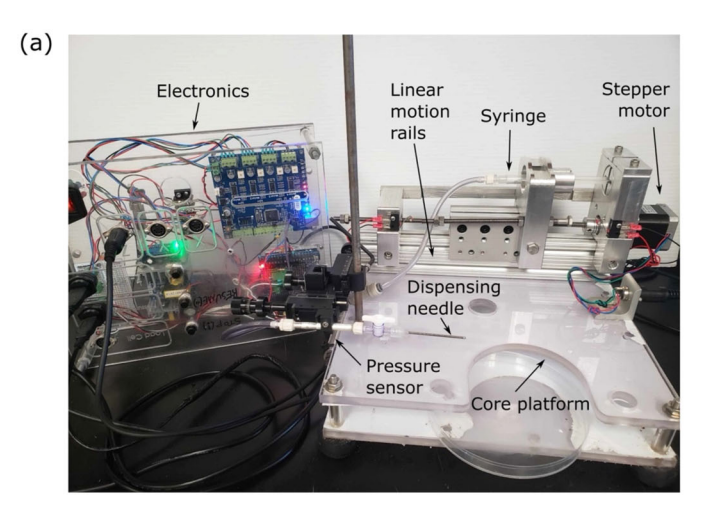
In this article, we present a bubble injection method to measure fracture toughness that uses side injection to obtain multiple measurements within a sediment core, resulting in a vertical depth profile with replicate measurements at each depth. Calculation of fracture toughness from measured pressure follows cavitation rheology theory (Kundu and Crosby 2009). In our experimental assessment of this method, we obtain visual confirmation of crack-shaped bubble formation in gelatin and natural sediments and compare the resulting values of fracture toughness to the range expected based on previous studies.

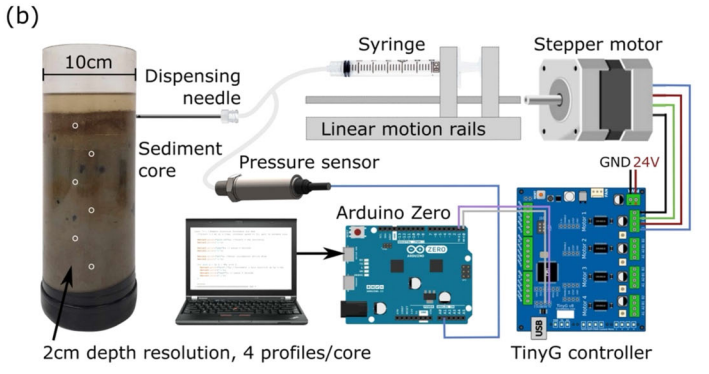
Theory and description of apparatus

Bubble growth and burrow extension by fracture are well predicted using linear elastic fracture mechanics (LEFM) theory. For both problems, fracture occurs when stress applied to the crack wall is amplified at the crack tip and exceeds the material property, fracture toughness, $K_{\rm Ic}$ (Pa m^{0.5}). $K_{\rm Ic}$ can be determined by initiating fracture through bubble formation and applying the LEFM solution for a disk-shaped crack.

The bubble injection instrument incrementally compresses air to increase pressure at the tip of a needle until a diskshaped bubble forms in the sediment sample by fracture at a critical peak pressure, P_c (Fig. 1c) (Barney et al. 2020; Anderson 2005).

$$P_{\rm c} = \sqrt{\frac{\pi E G_{\rm c}}{3R_{\rm in}}} \tag{1}$$





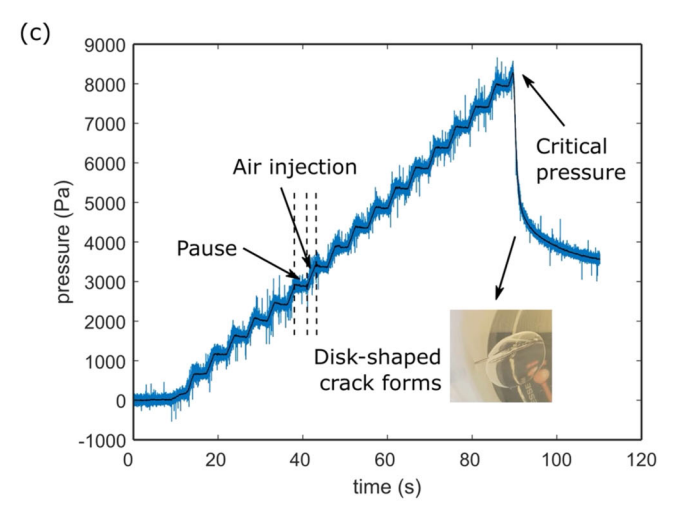


Fig. 1. (a) Image and (b) diagram of the bubble injection apparatus. (c) Pressure plot of bubble injection showing incremental air compression with the syringe until bubble is formed in muddy sediment at a critical peak pressure. A disk-shaped fracture bubble in gelatin is shown.

$$K_{\rm Ic} = \sqrt{\frac{EG_{\rm c}}{1 - (v)^2}} \tag{2}$$

Using Eq. 1, the pressure required to induce fracture bubble formation (P_c) depends on the radius of the needle, $R_{\rm in}$, and EG_c , Young's Modulus (Pa) multiplied by the critical energy release rate G_c (J m⁻²). Fracture toughness, as critical stress intensity factor, $K_{\rm Ic}$, can be calculated from EG_c following LEFM theory (Eq. 2) (Anderson 2005). Poisson's ratio, ν , is well approximated as ~0.5 for muddy marine sediments (L'Esperance et al. 2012).

The bubble injection apparatus forms fracture bubbles by using a syringe pump to build up air pressure through a needle inserted into the sediment. The syringe pump is a linear rail system assembled from a linear block bearing and custommachined parts that slide along a T-slotted aluminum extrusion to manipulate the position of a 3 mL syringe. A TinyG motion control board and a NEMA 17 bipolar stepper motor coupled with a threaded lead screw are used to control this motion (Fig. 1a,b). As the stepper motor is driven at a defined rate, the syringe piston is pushed forward to compress the air in the sealed system while a sensor measures the increasing pressure. When the pneumatic pressure through the needle reaches a critical point, the sediment fractures, and a diskshaped bubble of air forms (Fig. 1c). The fracture toughness is then calculated from the peak pressure at which fracture occurred (Eqs. 1 and 2; Barney et al. 2020). Both air and water have been used in cavitation rheology (Hutchens et al. 2016); we opted for air for simplicity in setting up the experiment.

Luer Lock fittings and tubing form a closed-air system including the syringe, needle, and a 15 PSI 4-20 mA pressure sensor. 14G (1.09 mm port diameter) and 22G (0.25 mm port non-coring needles are hamiltoncompany.com, Point Style 5), for mud and gelatin, respectively. Non-coring needles, with the dispensing port located on the side rather than at the tip, were used to prevent coring and clogging upon insertion. A smaller needle diameter requires higher pressure to induce fracture (Eq. 1), which either requires more time or a faster dispensing rate, but disturbs the material less upon insertion. Based on these considerations, needle sizes that worked well in each material were selected (Supporting Information Data S4). Various air injection rates were also tested, and no correlation between injection rate and the resulting K_{Ic} measurement was found (Supporting Information Data S4). Air injection rates for mud and gelatin were selected primarily based on the duration of the procedure.

The bubble injection procedure is automated and monitored using the Arduino computing platform. The TinyG stepper motor controller and pressure sensor are connected to an Arduino Zero microprocessor that executes user-prompted start and reset commands, provides real-time monitoring of the pneumatic pressure in the system through

the Arduino IDE Serial Plotter, and logs pressure sensor data to an SD card.

By starting at the top of a sediment core and injecting bubbles at increasing depths at 4 positions around the circumference of the core, a depth profile of fracture toughness with replicate measurements at multiple depths can be obtained, allowing for characterization of depth dependence and variability in fracture toughness.

Materials and procedures

Syringe pump

The syringe pump was constructed with custom aluminum parts and commercially available 80/20 linear motion products (Fig. 2a; Supporting Information Data S2). An 80/20 T-slotted aluminum extrusion frame (#1; Fig. 2a) acts as a guide rail to enable the linear operation of the syringe. The plunger end of the syringe is held fixed by the plunger mount (#5) and depressor clamp (#6), and the syringe body is pulled or pushed along the frame by the barrel holder (#3) mounted to the linear bearing (#2).

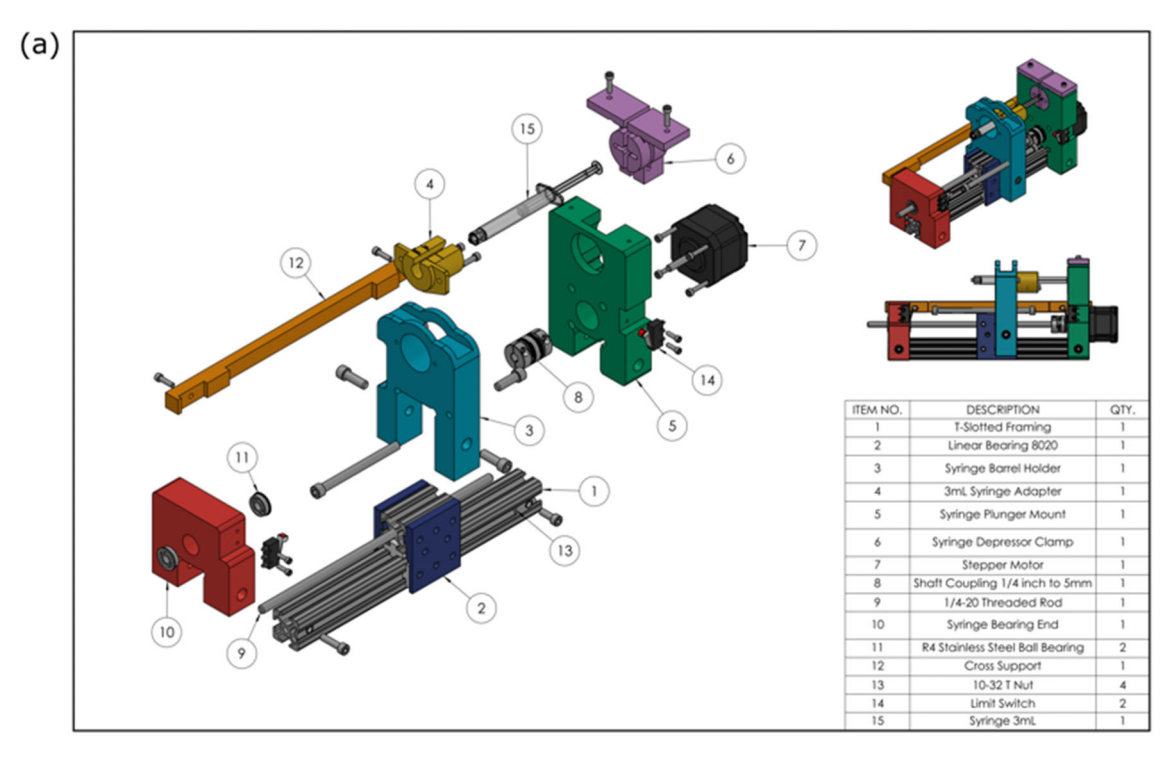
The rotation of a 1/4–20 lead screw (#9) running through the linear bearing drives the motion of the syringe barrel holder assembly along the frame. A NEMA17 stepper motor (#7) mounted to the plunger mount precisely controls this rotation. The lead screw connects to the stepper motor shaft via a shaft coupling (#8) and is supported on the other end of the assembly by the bearing end block (#10) and allowed to rotate by a ball bearing (#11). To provide a homing reference point for the syringe, a limit switch was placed flush against the side of the plunger mount (#14).

The syringe pump was designed to accommodate 5 mL and larger syringe sizes, but an adapter (#4) was made to hold a smaller 3 mL syringe to allow for more precision in volume dispensing control. The syringe barrel holder, 3 mL adapter, plunger mount, depressor clamp, bearing end, and cross support were machined from 6061 aluminum stock using a CNC milling machine (CAD files available at https://github.com/Anika-C/BubbleInjector), but could alternatively be 3-D printed or fabricated from other materials.

Electronics

The instrument is controlled with an Arduino Zero microcontroller (12-bit analog to digital converter) and a TinyG stepper motor controller, assembled in a control box powered by an 24 VDC AC/DC converter connected to a standard wall outlet plug (Fig. 2b; Supporting Information Data S2). The syringe pump limit switch, stepper motor, and 15 PSI 4-20 mA pressure sensor are connected to the control box through panel mount connectors.

The Arduino Zero receives 5 V power over USB from the user's computer and is fitted with an Adafruit SD card data logging shield and a screw shield for the pressure sensor circuit. The pressure sensor is wired to an analog input pin (A1) of the



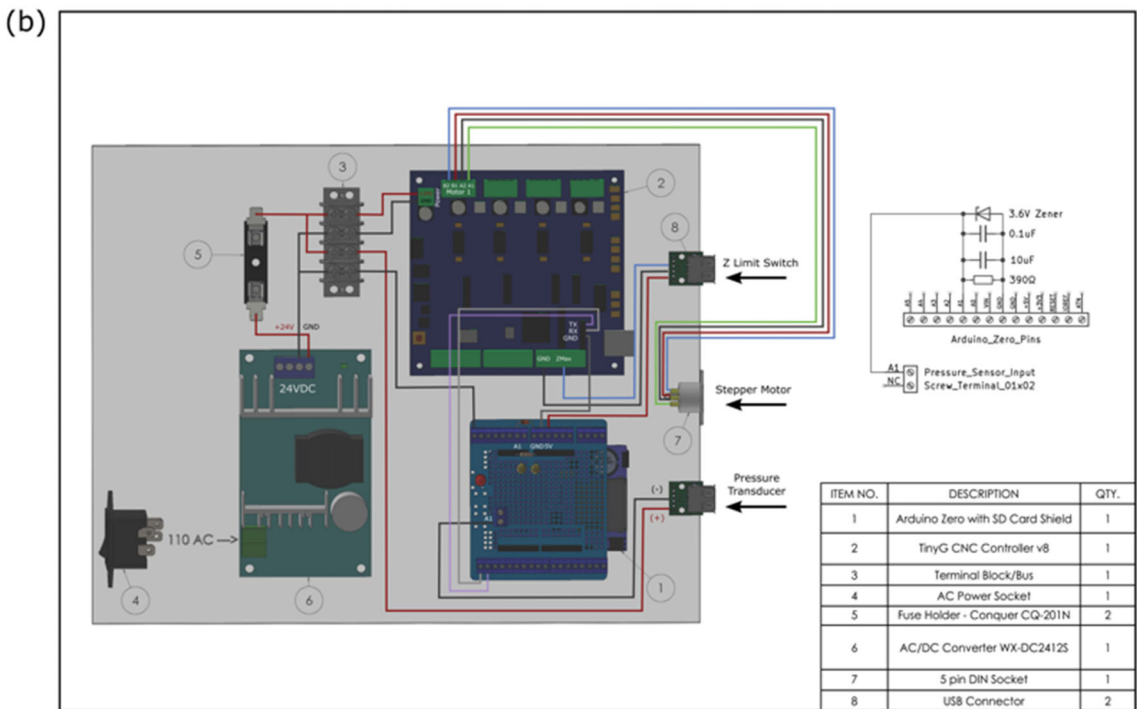


Fig. 2. (a) Syringe pump CAD model assembly. Component names and quantities provided in table and described in text. (b) Electronics control box layout and wiring schematic. All connections between the Arduino Zero microcontroller, TinyG CNC Stepper Motor Controller, pressure sensor, stepper motor, and syringe pump limit switch are shown and described in text. Connections from the pressure sensor to the analog input (A1) of the Arduino Zero are detailed in the schematic on the right.

Arduino Zero. The TinyG stepper motor controller and pressure transducer take 24 VDC from the AC/DC converter, and the Arduino Zero provides 5 V to the limit switch.

The stepper motor and limit switch are wired to the TinyG controller, and the TinyG controller and Arduino Zero are connected through the TX and RX pins. Calibration of steps

per air volume injected were controlled via the TinyG onboard settings (https://github.com/Anika-C/BubbleInjector).

General assembly

The syringe pump was mounted to a platform (constructed from ½" polycarbonate sheets) with a circular slot to hold a 10-cm-diameter sediment core in place during the bubble injection procedure (Fig. 1a). A 3-axis manual micromanipulator was mounted on a rod to hold the dispensing needle at adjustable heights. ½" OD tubing, Luer Lock fittings, and push-to-connect tee fittings were used to connect the syringe, pressure sensor, and needle to create a closed air system.

Before operating the instrument, the sediment sample is extruded into in a core with holes pre-drilled at the desired depths (here 2 cm resolution) and sealed with electrical tape on the outside of the core to prevent leaking. After inserting the needle at least 2 cm into the sediment sample through the electrical tape into one of the predrilled holes, the incremental air injection cycle is started through a serial command.

A complete list of the required materials and costs (Supporting Information Data S1), additional details on design considerations (Supporting Information Data S2), and a step-by-step procedure can be found in the Supporting Information Data S3.

Code

The Arduino code (Arduino 1.8.16) for the bubble injection procedure initiates preprogrammed sequences based on serial input from the user to reset the syringe position or begin automatic incremental air injection at specified rates for gelatin or mud (see Supporting Information Data S4). The changing pneumatic pressure within the syringe pump system is logged to the SD card and can be monitored through the Arduino Serial Plotter. When a sharp drop in pressure is observed, indicating fracture bubble formation, the reset button on the TinyG stepper motor controller can be used to end the air injection cycle. Data were plotted and $K_{\rm Ic}$ calculated using a custom Matlab script. All code and motor control settings are available on Github (https://github.com/Anika-C/BubbleInjector).

Assessment

To assess the effectiveness of the bubble injection instrument, it was important to verify consistent bubble formation by fracture and evaluate measurement accuracy and repeatability. In our experiments, we visually confirmed that crack-shaped bubbles formed in both gelatin and mud and took repeated $K_{\rm Ic}$ measurements in natural sediment samples for comparison with previous methods.

Indications and visualizations of bubble formation

Visual observations of bubble formation allowed us to verify that disk-shaped bubbles formed in both gelatin and natural sediments. Initial tests of the instrument were conducted in gelatin to observe bubble formation coinciding with a drop

in measured pressure. Bubbles could be easily visualized in gelatin (Fig. 1c) and consistently formed corresponding to pressure drops, as expected.

Although real-time visual observation of bubble formation was not possible in sediments, X-ray images of sediments taken shortly after bubble injection allowed us to verify our interpretation of pressure plots. To visualize cracks resulting from bubble injection in opaque natural sediments, bubbles were injected at 3 depths in 2 replicate 11.5 cm \times 2.5 cm rectangular cores of muddy sediment collected from the mouth of the York River, VA (37.2429 N, 76.3836 W), in October, 2022. Cores with fracture bubbles were then X-rayed with a MinXray HF100 high-frequency diagnostic unit at the Virginia Institute of Marine Science. Air bubbles were visible as a low density (dark-colored) region around the injection site (Fig. 3c-g). We expected pressure to increase as air was compressed by the actuation of the syringe, and for the pressure to fall when a bubble formed. This occurred in most cases, and the critical peak pressure, P_c , was clearly distinguishable (Fig. 3). In both of the X-ray cores, the fracture toughness increased with depth, requiring greater pressure to induce fracture. Both images also show more compacted (light-colored) sediment at depth.

In particularly compacted or deep sediments, there is occasionally no pressure drop, and no fracture bubble forms (Fig. 3e). The pressure is limited by the size of the 3 mL syringe to \sim 13.7 kPa, which places an upper limit on the measurable $K_{\rm Ic}$ of \sim 360 Pa m^{0.5} (Eqs. 1 and 2). The exact max pressure can vary slightly, potentially due to sediment heterogeneity or differences in air temperature and humidity. This limit was reached infrequently and can be resolved by increasing the syringe volume or increasing the needle diameter (see Eq. 1).

In most cases, the pressure drops from the critical pressure to a constant or slightly decreasing non-zero pressure. However, the injected bubble of air occasionally breached the surface of the sediment sample, resulting in a drop to zero pressure following the initial drop upon bubble formation (Fig. 3f). This primarily occurred when injecting bubbles in the upper 5 cm of sediment. The magnitude of the pressure drop varies considerably but did not show a clear pattern across depths and sediment types (data not shown). This variability likely reflects small-scale heterogeneity in sediments; when bubbles encounter zones of lower fracture toughness, the pressure drop would be larger (Boudreau 2012). Additional drops in pressure were occasionally observed after bubble formation (Fig. 3h), which we attribute to fracture bubbles expanding when they encounter burrows or weaker sediments.

Validation of fracture toughness measurements in sediments and gelatin

In preliminary testing of the instrument in natural muddy sediments during development, pressure dropped consistently, indicating bubble formation, but the values of fracture

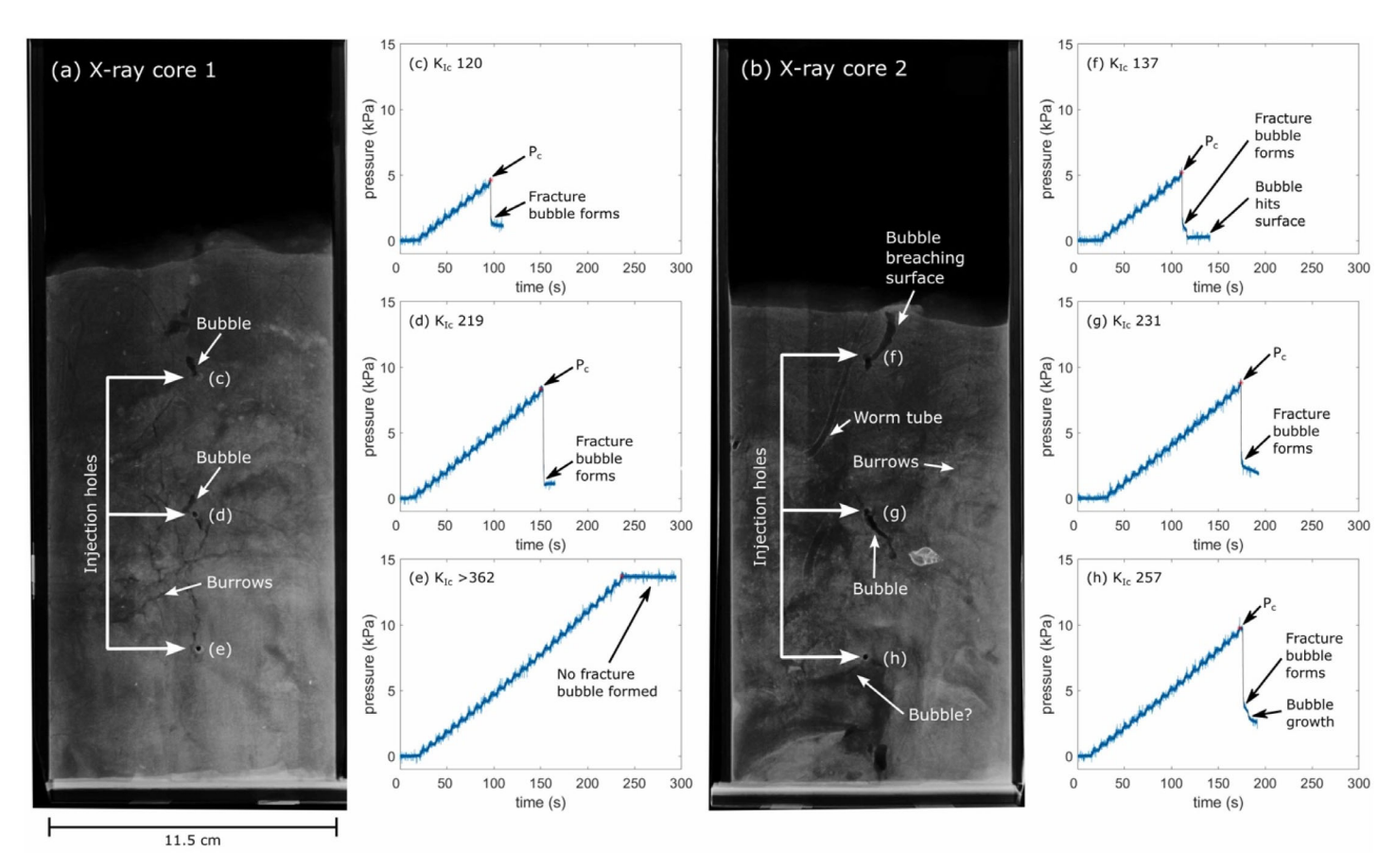


Fig. 3. (a,b) X-ray images of muddy sediment samples from York River, VA. (c-h) Bubble injection sites and their corresponding pressure plots are shown. K_{lc} values are given in Pa m^{0.5}.

toughness varied considerably. To better characterize this variability, replicate $K_{\rm Ic}$ measurements were taken at various depths in replicate cores of sediment and gelatin. We expected variability in homogeneous gelatin to reflect measurement error, and for variability in sediments to be greater and to reflect heterogeneity. We compared variability within vs. among sediment cores to better understand the scale of heterogeneity, and examined fracture toughness as a function of depth in both materials.

 $K_{\rm Ic}$ was measured via bubble injection in 10-cm-diameter cores of gelatin (www.bulkfoods.com, 28.35 g/L seawater; Dorgan et al. 2008) and cohesive, muddy sands collected from Mobile Bay, Alabama (30.25241 N, -88.01099 W) in June, 2022. Sediments from this site collected in June, 2021, were 90% sand, 10% mud, had porosity of 0.52, and exhibited cohesive behavior (site 14 from Dorgan et al. 2023). $K_{\rm Ic}$ measurements were taken at depths from 2 to 12 or 14 cm (2-cm intervals, 4 measurements per depth). $K_{\rm Ic}$ in gelatin did not vary with depth, and 68.1 ± 8.9 Pa m^{0.5} (mean \pm SD) compares well to previous measurements of 58.1 ± 8.2 Pa m^{0.5} and 65.4 ± 9.5 Pa m^{0.5} using two different methods of calculation (Dorgan et al. 2008).

 $K_{\rm Ic}$ of the sediment ranged from 50 to >360 Pa m^{0.5} (calculated from the max pressure given our syringe volume) (Fig. 4a). Previous measurements of $K_{\rm Ic}$ from cohesive sediments ranged from 280 to 490 Pa m^{0.5} at a depth of ~20 cm (Johnson et al. 2002). Our values fall within a plausible range, and, consistent with findings from Barry et al. (2013), fracture toughness increased gradually with depth.

It is important to note that replicate $K_{\rm Ic}$ measurements at constant depth in the same sediment core did not produce consistent values (Fig. 4b). In contrast, the $K_{\rm Ic}$ of gelatin was much more consistent with depth (Fig. 4a). Given that these measurements reflect fracture toughness on the scale of the needle diameter (1.09 mm), and sediments are known to be heterogeneous on these scales (Watling 1988), our observed variability is likely reflective of the heterogeneity of natural sediments rather than measurement error.

Discussion

Our bubble injection method appears to work well for assessing the fracture toughness of muddy sediments, producing results that are consistent with fracture mechanics theory

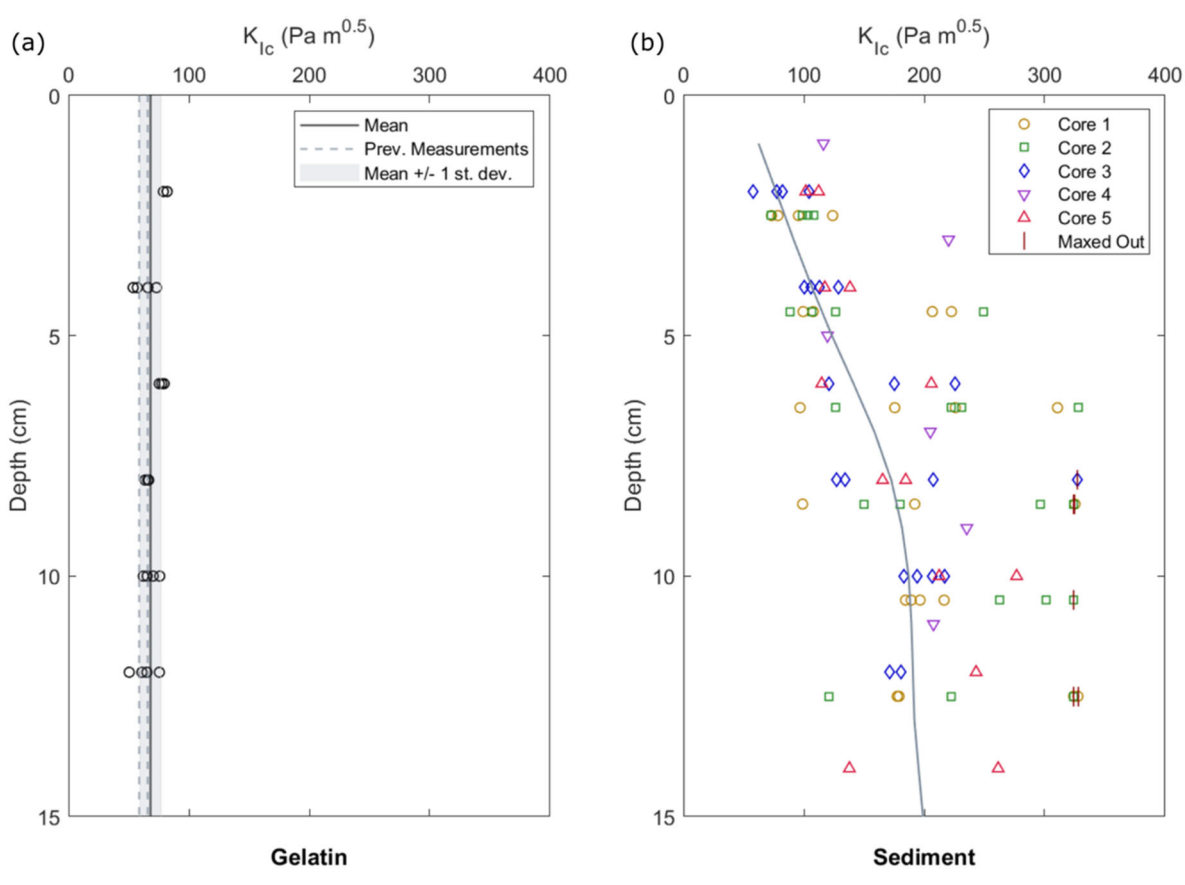


Fig. 4. (a) Bubble injection K_{lc} data ("o") for a gelatin core, with mean (solid line) and \pm one standard deviation (shaded), 68.1 ± 8.9 Pa m^{0.5}. Dashed lines indicate previous K_{lc} measurements in gelatin (Dorgan et al. 2008). (b) Bubble injection K_{lc} data from five sediment cores collected from a muddy sand site in Mobile Bay, AL. The line shows a smoothing spline fit. Injections in which no fracture bubble formed are plotted at \sim 360 Pa m^{0.5}, the max value, and highlighted with a red vertical line marker.

and align well with previous data from Johnson et al. (2002). Calculation of fracture toughness from the pressure corresponding to bubble initiation rather than over multiple iterations of bubble growth means that fracture toughness measurements are very small scale (1.09 mm), compared to measurements by Johnson et al. (2002) that calculated $K_{\rm Ic}$ from a series of bubble growth events. Our method allows for high spatial resolution data on how fracture toughness varies within marine sediments, as well as faster measurements and simpler analysis. Our higher spatial resolution data are likely also more variable, and our method may yield higher values of fracture toughness because the measurement is taken at a discrete point (the needle opening), whereas bubble growth follows the path of lowest fracture toughness.

This instrument can be used for assessing and quantifying heterogeneity in fracture toughness and, in combination with methods of visualizing density or compaction such as X-ray images or thin sectioning (Watling 1988), could provide greater insight into sediment heterogeneity. Johnson et al. (2002) attributed changes in the bubble growth behavior to sediment heterogeneity, but their method did not allow for quantification of variability in $K_{\rm Ic}$. A recent modeling study showed that

heterogeneity in fracture toughness leads to tortuosity and crack branching in the fracture paths of simulated burrowers and suggested that burrowers may steer burrows by creating crack branches and selecting a path (Dorgan and Arwade 2023). These results highlight the need for understanding and quantification of the variability in fracture toughness in natural sediments, which has not been explored. Characterization of heterogeneity with these localized, small-scale fracture toughness measurements can provide insight into where higher bioturbation rates (and therefore enhanced microbial productivity and nutrient cycling) are likely to occur in the seafloor. Direct comparison of the fracture toughness calculated from crack initiation with measurements following methods of Johnson et al. (2002) for crack growth may provide additional insight into sediment heterogeneity.

In contrast to the fracture probe developed by Johnson et al. (2012), where a corkscrew probe is screwed into the sediment and pulled up to break off a plug of sediment, bubble injection employs fluid (pneumatic) pressure to induce fracture. Similarly, burrowing worms exert fluid (hydraulic) pressure by pumping oxygenated water into their burrows. Thus, bubble injection may better represent the stresses applied

during burrowing. We found that fracture toughness measurements with the corkscrew probe method increase substantially with depth in sediment and that fracture appears more ductile with depth (Dorgan et al. 2024). Comparisons of measurements with these two methods could provide insights on how fluid pressure may influence burrowing mechanics. A disadvantage of both this bubble injection method and our modified corkscrew probe (Dorgan et al. 2024) is that both are laboratory rather than in situ measurements.

This method is also currently limited to muddy sediments that fail by fracture under tensile stresses. While our X-ray images (Fig. 3) and previous studies have shown that bubbles in muds are disk-shaped cracks (Johnson et al. 2002; Boudreau et al. 2005), bubbles in non-cohesive sands are spherical and do not form by fracture (Boudreau et al. 2005). Discrete element modeling of bubble migration shows a shift in mechanics from fracture to capillary invasion with increasing grain size (Jain and Juanes 2009). On the other extreme, in very soft muds, it is possible that bubbles might form by cavitation rather than fracture, in which case peak pressure values would not accurately predict fracture toughness (Barney et al. 2022). The resulting spherical shape is inconsistent with growth rates or shapes of bubbles in natural sediments (Boudreau 2012). Our calculations indicate that the transition from fracture to cavitation would occur at a ratio of stiffness to fracture toughness more than two orders of magnitude lower than previous measurements in natural sediments. Thus, this mechanism is unlikely a substantial concern, but cannot be completely discounted (see Supporting Information Data S5). While bubble formation could be clearly observed in gelatin, sediments are opaque, making it difficult to confirm that disk-shaped bubbles form. Modifications to the fracture probe developed by Johnson et al. (2012) have shown a clear transition in fracture behavior from muds to sands, with muds showing tensile strength and elastic behavior and sands showing a lack of cohesion (Dorgan et al., 2024). In this study, bubbles were only injected in muds known to exhibit cohesive behavior (Dorgan et al., 2023), therefore all observed pressure drops were considered as fracture bubbles. Further testing with both methods is needed to better characterize the range of natural sediments in which fracture occurs.

Comments and recommendations

Several modifications could be made to the bubble injector apparatus to improve performance and simplify the operating procedure. The maximum pressure of the current system is too low to measure the full $K_{\rm IC}$ range of marine muds, so bubbles occasionally are not formed in deeper, more cohesive sediments. Since these data were collected, this has been resolved by switching to a larger volume syringe. The vertical depth resolution of the instrument could also be improved by adding more closely spaced insertion holes to the sample cores,

although this would also increase the time to process a single core (currently \sim 2 h for 20 bubbles).

Automation could also simplify and shorten the bubble injection procedure. The manual height adjustment and needle insertion mechanisms could be automated to speed up sample collection. Currently, the needle is removed and rinsed between injections to prevent clogging; automation to achieve multiple bubble injections would require additional needles and components. The code could be modified to detect a sharp pressure drop (bubble formation) and automatically end the air injection cycle, reducing the time and attention required from the operating technician. A challenge is that the magnitude of the pressure drop varies considerably.

Future development of an in situ version of the instrument for marine sediments would eliminate the disturbance of collecting and transporting cores and allow for more accurate measurements. Development of an in situ bubble injection system would require modification of the pneumatic system to be used underwater as well as measurement of differential pressure that accounts for changes in the ambient pressure, e.g., from waves.

References

Anderson, T. L. 2005. Fracture mechanics, 3rd Edition. CRC Press, p. 621.

Barney, C. W., C. E. Dougan, K. R. McLeod, and others. 2020. Cavitation in soft matter. Proc National Acad Sci **117**: 9157–9165. doi:10.1073/pnas.1920168117

Barney, C. W., I. Sacligil, G. N. Tew, and A. J. Crosby. 2022. Linking cavitation and fracture to molecular scale structural damage of model networks. Soft Matter **18**: 4220–4226. doi:10.1039/d2sm00400c

Barry, M. A., B. D. Johnson, B. P. Boudreau, B. A. Law, V. S. Page, P. S. Hill, and R. A. Wheatcroft. 2013. Sedimentary and geo-mechanical properties of Willapa Bay tidal flats. Cont. Shelf Res. **60S**: S198–S207. doi:10.1016/j.csr.2012. 05.007

Boudreau, B. P. 2012. The physics of bubbles in surficial, soft, cohesive sediments. Mar. Pet. Geol. **38**: 1–18. doi:10.1016/j.marpetgeo.2012.07.002

Boudreau, B. P., and others. 2005. Bubble growth and rise in soft sediments. Geology **33**: 517. doi:10.1130/g21259.1

Daigle, H., A. Cook, Y. Fang, A. Bihani, W. Song, and P. B. Flemings. 2020. Gas-driven tensile fracturing in shallow marine sediments. J. Geophys. Res. Solid Earth **125**: e2020JB020835. doi:10.1029/2020JB020835

Dorgan, K. M., P. A. Jumars, B. D. Johnson, B. P. Boudreau, and E. Landis. 2005. Burrow extension by crack propagation. Nature **433**: 475. doi:10.1038/433475a

Dorgan, K. M., S. R. Arwade, and P. A. Jumars. 2008. Worms as wedges: Effects of sediment mechanics on burrowing behavior. J. Mar. Res. **66**: 219–254. doi:10.1357/002224008785837130

- Dorgan, K. M., S. Lefebvre, J. Stillman, and M. A. R. Koehl. 2011. Energetics of burrowing by the cirratulid polychaete *Cirriformia moorei*. J. Exp. Biol. **214**: 2202–2214. https://doi.org/10.1242/jeb.054700
- Dorgan, K. M., and S. R. Arwade. 2023. Material properties of sediments steer burrowers and effect bioturbation. J. Geophys. Res. Biogeosci. **128**. doi:10.1029/2022jg007269
- Dorgan, K. M., and others. 2023. Relating tensile strength to other sediment properties along a sand-mud gradient in Mobile Bay, Alabama. Coast. Sediments **2023**: 1565–1575. doi:10.1142/9789811275135_0145
- Dorgan, K. M., G. Lockridge, and W. C. Clemo. 2024. Small-scale measurement of the transition in fracture behavior of marine sediments. Acta Geotech. **19**: 1315–1326. https://doi.org/10.1007/s11440-023-02134-6
- Hutchens, S. B., S. Fakhouri, and A. J. Crosby. 2016. Elastic cavitation and fracture via injection. Soft Matter **12**: 2557–2566. doi:10.1039/c5sm02055g
- Jain, A. K., and R. Juanes. 2009. Preferential mode of gas invasion in sediments: Grain-scale mechanistic model of coupled multiphase fluid flow and sediment mechanics. J. Geophys. Res. Solid Earth 114: B08101. doi:10.1029/2008jb006002
- Johnson, B. D., B. P. Boudreau, B. S. Gardiner, and R. Maass. 2002. Mechanical response of sediments to bubble growth. Mar. Geol. **187**: 347–363. doi:10.1016/s0025-3227(02)00383-3
- Johnson, B. D., M. A. Barry, B. P. Boudreau, P. A. Jumars, and K. M. Dorgan. 2012. In situ tensile fracture toughness of surficial cohesive marine sediments. Geo-Mar. Lett. 32: 39– 48. doi:10.1007/s00367-011-0243-1
- Kundu, S., and A. J. Crosby. 2009. Cavitation and fracture behavior of polyacrylamide hydrogels. Soft Matter **5**: 3963. doi:10.1039/b909237d

- L'Esperance, J. C., B. P. Boudreau, M. A. Barry, and B. D. Johnson. 2012. Small-scale, high-precision and high-accuracy determination of Poisson's ratios in cohesive marine sediments. Geo-Mar. Lett. **33**: 75–81. doi:10.1007/s00367-012-0305-z
- Meysman, F., J. Middelburg, and C. Heip. 2006. Bioturbation: A fresh look at Darwin's last idea. Trends Ecol. Evol. **12**: 688–695. doi:10.1016/j.tree.2006.08.002
- Watling, L. 1988. Small-scale features of marine sediments and their importance to the study of deposit-feeding. Mar. Ecol. Prog. Ser. **47**: 135–144. doi:10.3354/meps047135

Acknowledgments

The authors thank Maddy Frey, Cy Clemo, and Moey Rojas for their assistance with sediment collection from Mobile Bay. Grace Massey and Harrison Kempton helped with sample collection and took X-ray images of sediments from the York River. This project benefitted from helpful discussions with Al Crosby about cavitation rheology and the feasibility of applying his methods to marine sediments. We also gratefully acknowledge the GrabCAD community for the commercial off-the-shelf parts models used in our CAD assemblies. Funding for this project was provided by the National Science Foundation (NSF REU Grant #2150347), the Office of Naval Research (ONR Grant #N00014-20-1-3477 and #N00014-21-1-2214), and DoD SERDP award MR21-C1-1265. This project was also supported through the US Naval Research Lab's Base Program Funding.

Submitted 06 December 2023 Revised 22 April 2024 Accepted 29 April 2024

Associate editor: Paul F. Kemp